Available online at www.eccomasproceedia.org
Eccomas Proceedia SMART (2023) 1743-1754

ECCOMAS
Proceedia

X ECCOMAS Thematic Conference on Smart Structures and Materials
SMART 2023
D.A. Saravanos, A. Benjeddou, N. Chrysochoidis and T. Theodosiou (Eds)

SPATIALLY RESOLVED STRAIN MEASUREMENT AT METER SCALE USING A CARBON FIBER BASED STRAIN SENSOR AND ARTIFICIAL NEURAL NETWORKS

N. WIEJA*, P. J. STEINBILD*, T. EHRIG*, A. WINKLER*, P. KOSTKA*, J. CONDÉ-WOLTER*, N. MODLER*,

*Institute of Lightweight Engineering and Polymer Technology, TU Dresden, Germany
e-mail: nils.wieja@tu-dresden.de

Key words: carbon fiber, composite, continuous strain measurement, spatially resolved strain sensor, convolutional neural network, structural health monitoring

Abstract. Life cycle optimization, maintenance planning and adaptive control systems in fiber-reinforced structures such as aircraft wings require the monitoring of loads and stresses during operation. State of the art systems using strain gauges can measure strains at limited numbers of discrete points, while systems based on fiber optic time domain reflectometry require complex and cost intensive evaluation units. A novel sensor based on electrical time domain reflectometry (ETDR) allows to acquire information about the spatial distribution of strain along a fractured carbon fiber (CF) embedded in a composite structure. This sensor concept has been investigated in previous studies with specimens up to 60 mm in length. Based on this work, a demonstrator with an improved sensor layout and two embedded sensors of 1 m length is developed. A shallow feed-forward network and a convolutional neural network are compared regarding their ability to infer strain profiles from measured ETDR reflectograms. The simultaneous evaluation of two sensors with a convolutional neural network allowed the inference of strain distributions with a good generalization ability.

1 INTRODUCTION

Structural health monitoring of highly stressed lightweight structures is key to achieve further weight reduction and life cycle optimization, both enabling resource-efficient products [1]. This can be achieved by a continuous in operando measurement of loads and strains, which also enables active load reduction when evaluated in real time. Commonly used systems are based on strain measurements, which can be performed using different measurement principles. While state of the art systems such as strain gauges and fiber Bragg grating allow strain measurements at a limited number of points, the monitoring of large structures requires numerous measurement points. Optical measurement systems using time domain reflectometry (OTDR) allow a continuous strain measurement along an embedded optical fiber. A series of probe pulses is fed into the optical fiber, where various attenuation effects cause a fraction of the light to be guided back to the launching end. This backscattered light is then detected and processed. It contains

Peer-review under responsibility of the organizing committee of SMART 2023.
doi: 10.7712/150123.9945.444359

information about the properties of the fiber that affect attenuation, such as strain and temperature, which can be spatially resolved, considering the signal propagation time [2]. While optical fibers can be easily integrated into composite structures, the necessary instrumentation is typically cost intensive and requires significant installation space. This limits current application mainly to experimental setups, civil structures and geophysical monitoring [3]. Conventional data processing methods use curve fitting methods to calculate temperature and strain profiles from the detected backscatter signature of an OTDR measurement. These methods require a large number of data points, expensive computation, and are sensitive to measurement noise. Recently, the use of artificial neural networks (ANN) has been adopted for the analysis of OTDR data, enabling real-time applications and enhancing robustness to noise [4, 5].

A novel sensor principle proposed by Höhne et al. [6] shows the potential to realize a distributed strain measurement in FRP structures based on a miniaturizable and relatively inexpensive technology. The principle, as shown in figure 1, is based on an ultra high modulus (UHM) carbon fiber (CF) roving that is embedded in a glass fiber reinforced polymer (GFRP) carrier. In a tensile test, the structure is then deliberately loaded beyond the maximum strain of the CF roving, resulting in multiple fiber cracks along the CF roving, while the carrier structure remains intact due to it's highter ultimate elongation. This process is referred to as "functionalization". The functionalized CF roving shows a high sensitivity of its resistance to applied strain due to the opening and closing of the fiber cracks. Spatially resolved strain sensing along the CF-roving can be achieved using electrical time domain reflectometry (ETDR). This is facilitated by adding a copper strip as a return conductor to the structure to form a transmission line (TL) with the CF. An ETDR instrument transmits an incident step signal into a TL and acquire the resulting reflections. The signal propagating along the TL is partially reflected by impedance variations along the TL. Considering the signal propagation time, incoming reflections can be spatially resolved. The reconstruction of spatially resolved electrical properties from ETDR-reflectograms by solving an inverse electromagnetic problem (IEP) has been the subject of research [7, 8], which identifies high computational cost and lack of robustness to measurement noise as remaining limitations. In the specific case of the strain sensor described, the stochastic nature of the fiber cracks and the lack of comprehensive models describing their electric properties further limit the applicability of conventional processing methods. To overcome this, Höhne et al. [9] suggested the use of ANNs to derive strain profiles from the measured reflectograms. The methodology was demonstrated using a GFRP cantilever beam of 60 mm length with an embedded sensor. 136 different load cases were generated through variation of the clamping position and applied load. A shallow ANN with 32 input neurons, 32 hidden neurons and 8 output neurons, representing the strain on equidistant points of the cantilever beam, was trained on 126 load cases, with strain profiles calculated analytically. The ANN's prediction for the test data agreed well with the calculated strain profiles, though the authors suggest an automation of training data generation to increase the amount and quality of the training data. The present article describes a further development of the sensor concept presented by Höhne et al. [9] and demonstrates its applicability to measuring lengths in the range of one meter, driven by the goal of an implementation in sailplane wings [10]. Possible load conditions are expanded by a novel sensor design using two CF rovings on either side of a beam structure to detect bending in both directions. To generate sufficient training data, a test bench is developed, and the acquired data is used to train and compare different ANNs with regard to their generalization abilities.

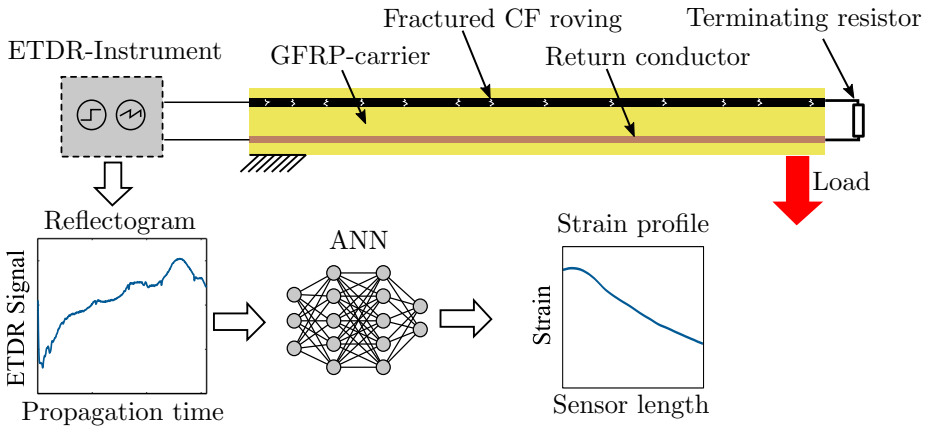

Figure 1: Principle of the strain sensor and evaluation process described by Höhne et al. [9]

2 MATERIALS AND METHODS

The demonstrator structure presented in this work was developed with the goal of being able to apply as many load cases as possible without changing the clamping to allow a simple collection of training data. Since the fractured CF-rovings are mainly sensitive to tensile strain, CF-rovings were embedded on both sides of a bending beam structure in order to sense bending in both directions. Target values for the training of ANNs were obtained from the elastic curve of the beam.

2.1 Design and manufacturing process

The specimen was designed as a flat bar with dimensions of 1200 mm length, 30 mm width and 2.8 mm thickness. To ensure proper clamping, cap strips are applied to each end of the bar. A free length of 1000 mm between the cap strips is used for strain measurement. The sensor elements are contacted outside the free length to ensure an undisturbed structure. The geometry of the specimen is depicted in figure 2. The structure was manufactured in an autoclave process using glass-fiber reinforced epoxy prepreg material (Unidirectional prepreg Krempel GUBD 2506). A plate with integrated sensor elements was made from 14 layers of prepreg in a stacking sequence of $[0°/\mathrm{CF}/0°/90°/90°/0°/90°/0°/\overline{\mathrm{Cu}}]_\mathrm{S}$, where $\overline{\mathrm{Cu}}$ represents the midplane copper strip and CF the embedded CF-rovings. The CF-roving was embedded between two 0° layers to prevent the fibre cracks from propagating into the GFRP-carrier. The thickness of 1.2 mm between CF and copper strip was chosen to match the impedance of the TL with the measurement systems impedance of 50 Ω. The type of CF used is Mitsubishi Dialead K13C2U with a filament count of 2000, the copper foil tape has a width of 6 mm and a thickness of 0.035 mm. The CF-rovings were contacted with coaxial cables (type RG 178) at both ends of the specimen using silver-filled conductive epoxy (MG Chemicals 8330S-21G), the braid of the coaxial cables was soldered to the copper foil tape that acts as return conductor for both CF-rovings. A plate of the described laminate was cured at 120 °C with an effective pressure of 7 bar. The specimen was then prepared by waterjet cutting.

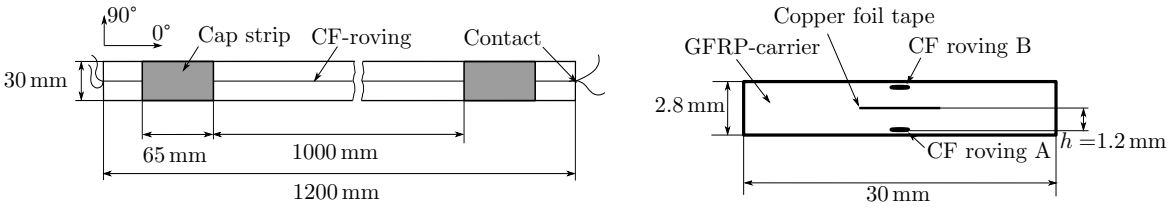

a) Outer dimensions of the developed specimen

b) Cross-section of the developed specimen without cap strips

Figure 2: Geometry of the developed specimen (not to scale)

2.2 Functionalization

In order to achieve a distribution of fiber cracks in the CF-rovings along the entire length of the specimen, the structure was sectionally loaded in a 4 point bending test. A load span of 27 mm and a support span of 81 mm were chosen in accordance with ISO 14125 [11]. The specimen was segmented into 35 sections of 27 mm length that were loaded in both directions to a deflection of 5.65 mm which corresponds to a strain of approximately 0.95 % in the CF roving. For each section and both directions, the load was applied cyclically with a test speed of 10 mm min^{-1} in the first cycle and 100 mm min^{-1} in following cycles. The test setup is depicted in figure 3a. During the functionalization, the resistance of both CF-rovings was measured using a custom ohmmeter. Figure 3b shows an example of the resistance of both rovings during a functionalization cycle of Roving B (tension). Roving A (compression) has previously been functionalized in the corresponding section. The resistance of each roving is referred to the base resistance R_0 of 23.7 Ω (Roving A) respectively 20.2 Ω (Roving B) measured at the beginning of the test. The roving loaded with tension shows a nonlinear increase of its resistance with the applied force, while the resistance of the roving experiencing pressure load shows a negative change at the beginning of each cycle but does not change with a further increasing load.

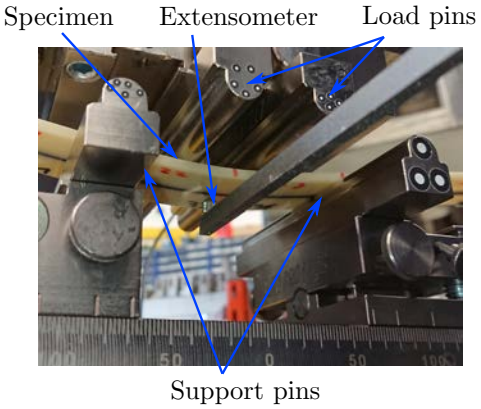

a) Setup used for functionalization of the specimen

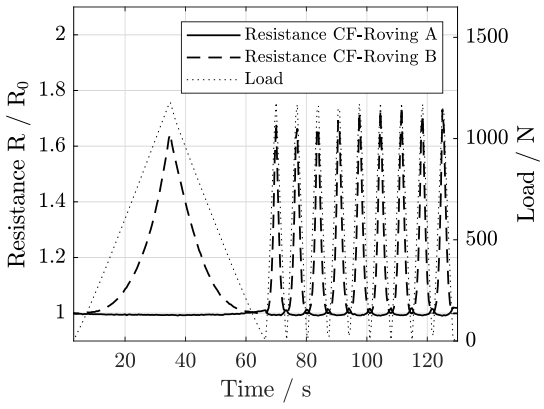

b) Measured resistance of the CF-rovings during functionalization

Figure 3: Test setup and measured resistance during functionalization

The functionalization process led to fiber cracks with a spacing of approx. 1-2 mm, surrounded by light discoloration, most likely due to local delaminations. A section of a CF roving after functionalization is shown in Figure 4. Fiber cracks in the CF-roving are visible between lighter discolorations, one of the visible fiber cracks is marked as an example. Note that the visible white lines are caused by surface imperfections due to the manufacturing process.

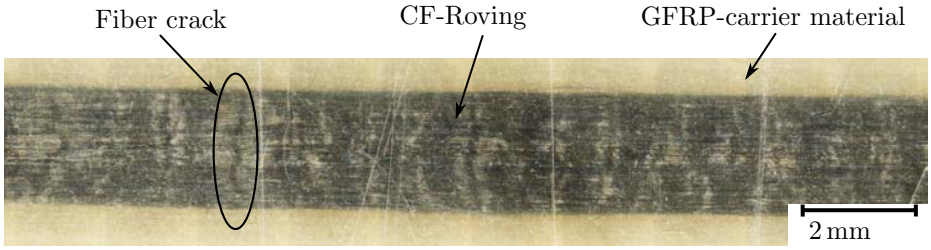

Figure 4: Fracture pattern of a CF-roving after functionalization with one fiber crack marked as an example

2.3 Acquisition of Training Data

In order to obtain training data for a wide range of load cases, a test bench that allows the setting of different bending conditions by applying bending angles at both ends of the structure was developed. The test bench is depicted in figure 5. A floating bearing was realized by a linear guide to eliminate longitudinal loads. Bending angles can be set using detent bolts on both sides. The resulting elastic curve of the specimen is optically captured with a camera and fitted with a spline function in the xy coordinate system of the image. The curvature κ is then calculated by solving the differential equation [12]

$$\kappa = \frac{\frac{\mathrm{d}^2 y}{\mathrm{d}x^2}}{\left(1 + \left(\frac{\mathrm{d}y}{\mathrm{d}x}\right)^2\right)^{3/2}} \tag{1}$$

numerically. Using

$$l(x) = \int_0^x \sqrt{1 + \left(\frac{\mathrm{d}y}{\mathrm{d}x}\right)^2}\,\mathrm{d}x \tag{2}$$

the curvature is transformed to the longitudinal coordinate l of the specimen [13]. Furthermore, $\varepsilon = d \cdot \kappa$ is assumed for the relation between the curvature κ and the strain ε at an offset d to the neutral axis.

ETDR measurements were performed with a Sympuls D-TDR 3G-500 instrument. It allows dual channel measurements with a resolution of 500 sampling points at a frequency of 1000 Hz. One end of the sensors was connected to the instrument using SMA connectors and the other end of each sensor was terminated with a 50 Ω resistor. A total of 746 load cases were generated by gradually changing the bending angles on both sides. Due to friction in the linear guide, two

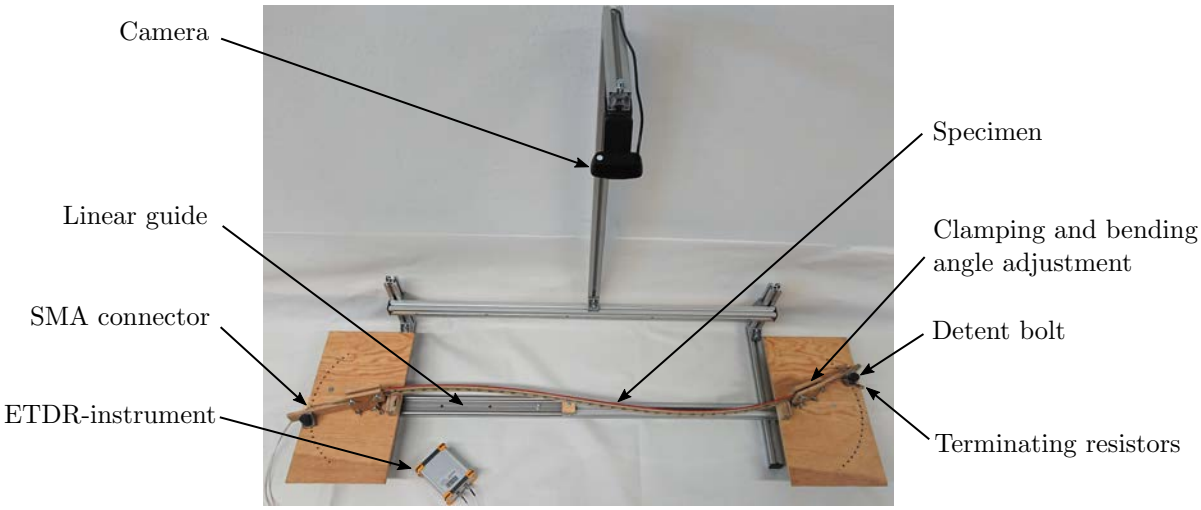

Figure 5: Test bench used to generate training data

load cases with slightly different elastic curves were generated for each combination of detent bolt positions. Additional 171 load cases were generated by applying transverse load at various positions along the free length of the specimen using a lashing strap. For each load case applied, 500 dual channel ETDR measurements with a resolution of 500 sampling points were performed, and an image of the bend specimen was captured. The acquired data was separated into four sets for the training and testing of ANNs according to the scheme in figure 6. The first 672 signal recordings generated by gradual changes of the bending angels were used in the training process of ANN for training (90 %) and validation during the training process (10 %). Load cases generated by further changes of the bending angles were used as a first level test data. Due to the gradual change of the bending angles, the elastic curves in this data set differ systematically from the training data. The 171 load cases generated with an additional transverse load were used as second level test data. For the training of ANNs, the curvature κ at 50 equidistant points along the specimen's longitudinal coordinate l was used as target values. The 500 measurements per channel acquired for each load case were averaged to achieve a low noise signal and were normalized to $[0, 1]$ before training.

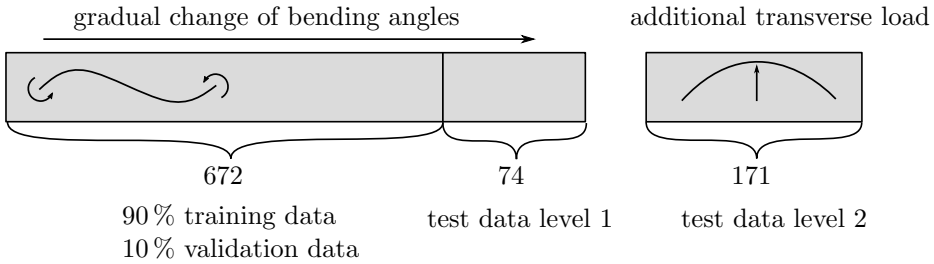

Figure 6: Scheme for the split of the acquired data for training, validation and testing

2.4 Description of the studied ANN

Two ANNs with different architectures were studied for the evaluation of the acquired ETDR-data: A shallow, fully connected feed-forward network (FNN) similar to the ANN used by Höhne et al. [9] to evaluate CF-Strain sensors and a convolutional neural network (CNN). In both cases, the ANNs were designed to perform a regression for the curvature κ at 50 equidistant points along the specimen, each represented by one output neuron. The architecture of both ANNs is depicted in figure 7. To compare the performance of different ANNs, the root mean square error (RMSE) between the target values and the ANN predictions for the respective data sets is considered.

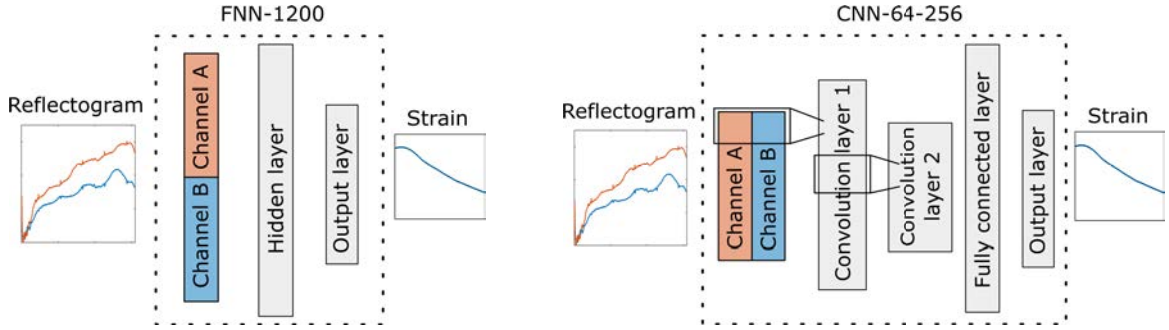

a) Schematic of FNN-1200 **b)** Schematic of CNN-64-256

Figure 7: Schematic depiction of the studied ANNs

2.4.1 FNN-1200

The studied FNN was designed with a 1000 neuron input layer. The measurements from both channels were concatenated and fed into the FNN. The effect of the number of neurons in the hidden layer on the performance of the ANN was evaluated in several iterations, and an optimized number of 1200 neurons with hyperbolic tangent (tanh) activation function was chosen. The output layer was designed with 50 neurons representing the curvature of the specimen at 50 equidistant points. The described architecture is depicted in figure 7a. This neural network (referred to as FNN-1200) was trained using the Adam algorithm [14] implemented in Matlab R2022a, with an initial learning rate of 0.002, which was reduced by half every 50 epochs. The training data was processed in mini-batches of 32 load cases, and the training was terminated once the mean squared error for the validation data set did not improve after 1000 iterations.

2.4.2 CNN-64-256

The studied CNN was designed with two convolutional layers, each followed by a max pooling layer. The measured values were fed into an 500×2 input layer. The first convolutional layer was designed with 64 filters of kernel size 31×2, the second convolutional layer with 256 filters of kernel size 15×1. Both layers were designed with stride 2 and ReLU activation function and followed by a 3×1 max pooling layer. The convolutional layers are followed by one fully

connected layer with 1000 neurons and tanh-activation and an output layer with 50 neurons. The described architecture is depicted in figure 7b. This ANN (referred to as CNN-64-256) was trained using the Adam algorithm with an initial learning rate of 0.001, which was reduced by half every 80 epochs. As with FNN-1200, a mini-batch size of 32 was used, and the training was terminated once the mean squared error for the validation data set did not improve after 1000 iterations.

3 RESULTS

3.1 Evaluation of the signal sensitivity to homogeneous strain distribution

The beginning and the end of the sensor in the time domain were determined from the reflectograms of the unloaded sensors, as shown in figure 8. Characteristic elements of the obtained TDR signal such as the signal generator (a), the SMA connectors on both sides of the specimen (b, d) and the contact between the coaxial cables and the sensors elements (c) can be located in the reflectogram. A signal propagation time of 15.5 ns over the length of the specimen was determined.

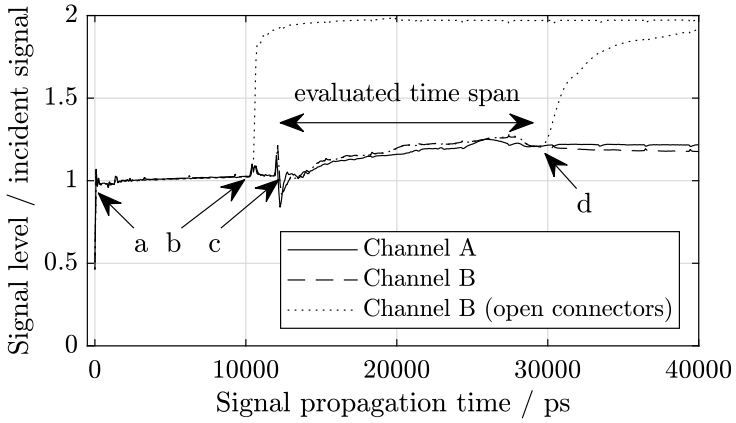

Figure 8: Measured ETDR-Signal for the test setup with unloaded specimen. a) Signal generator, b) SMA connector, c) contact between cable and sensor, d) SMA connector with terminating resistor

The influence of strain on the obtained ETDR-signal of Channel A is shown in figure 9. To generate the reflectograms, the specimen was loaded with a constant strain by applying identical bending angles on both sides. This was repeated to achieve tension and compression loads of the same roving. The measured reflectograms are compared with the the unloaded roving. Both, tension and compression strains appear to affect the resulting ETDR signal, with compression reducing the signal level and tension increasing it. At the applied strain magnitude of 0.25 %, the shift due to compression is less than that observed during tensile loading. This corresponds to the change in resistance during the functionalisation cycles shown in figure 3b.

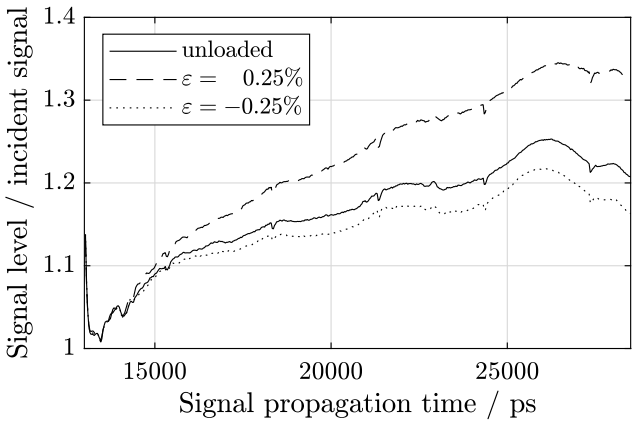

Figure 9: Variation of the obtained ETDR signal of one CF-roving in the evaluated time span at constant tension and compression load

3.2 Evaluation of reflectograms with artificial neural networks

The achieved RMSE of FNN-1200 and CNN-64-256 for the different data sets are summarized in table 1. While FNN-1200 shows a smaller RMSE of $0.183\,\mathrm{m}^{-1}$ compared to CNN-64-256 ($0.224\,\mathrm{m}^{-1}$) for the training data, both ANNs perform similar on the validation data with a RMSE of $0.263\,\mathrm{m}^{-1}$ and $0.269\,\mathrm{m}^{-1}$. However, for both levels of test data, CNN-64-256 showed a significantly lower RMSE of $0.949\,\mathrm{m}^{-1}$ and $1.377\,\mathrm{m}^{-1}$, compared to $1.907\,\mathrm{m}^{-1}$ and $2.201\,\mathrm{m}^{-1}$ for the predictions of FNN-1200. The difference between the RMSE for the training and validation data sets observed for FNN-1200 indicates the ANN's tendency to overfit the training data. Accordingly, it showed higher RMSE for the test data sets. CNN-64-256 on the other hand produced slightly higher RMSE for the validation and especially the training data but clearly outperformed FNN-1200 on the test data sets, which indicates a better generalization ability. To illustrate the relation of the RMSE-values and its effect on the measured curvarures, figure 10 shows exemplary predictions of both ANNs for selected load cases from the validation and test data sets. Especially for level 2 test data, FNN-1200 generates an erratic output, while the estimated curvature of CNN-64-256 appears smoother.

Table 1: Comparison of the RMSE of FNN-1200 and CNN-64-256 for the different data sets

ANN	RMSE in m^{-1}			
	Training	Validation	Test Level 1	Test Level 2
FNN-1200	0,183	0,263	1,907	2,201
CNN-64-256	0,224	0,269	0,949	1,377

The networks training, as well as the resulting RMSE for the different data sets, were obtained by averaging 500 ETDR measurements before feeding the resulting reflectogram into the ANNs. Since the measurement rate of ETDR devices is limited, it is necessary to process reflectograms averaged from fewer individual measurements to further increase the strain measuring rate. This consequently results in a higher level of input noise for the ANNs. The input noise sensitivity of

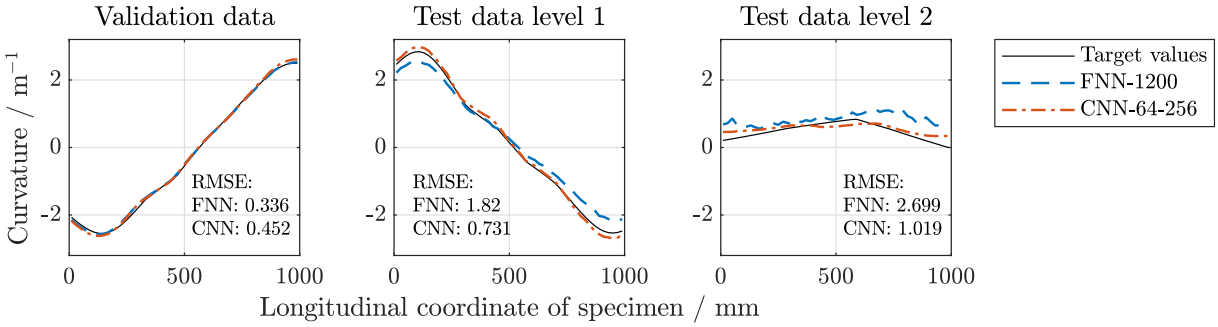

Figure 10: Exemplary illustration of curvatures predicted with FNN-1200 and CNN-64-256

FNN-1200 and CNN-64-256 was studied by evaluating their performance for input data averaged from different numbers of individual measurements. The previously described data sets with their particular loadcases were used, but the number of averaged ETDR measurements for each loadcase was varied from 1 to 500. The resulting RMSE are depicted in figure 11. The values shown for 500 averaged measurements reflect the values in table 1. As the noise increases, the resulting RMSE for the load cases in the training data set is increased, but is still lower than for the test data sets. The RMSE of the validation data set decreases to the level of the training data when the number of averaged measurements is reduced to 250 and shows equivalent values to the training data set with further increasing noise levels. The errors for the test data remain at a constant level, except when single ETDR measurements are used as input data. Overall, the performance of the ANNs decreases with increasing input noise, especially for the training and validation data sets. This decrease is more prominent for FNN-1200 than for CNN-64-256, which can be attributed to the better generalization ability of the latter.

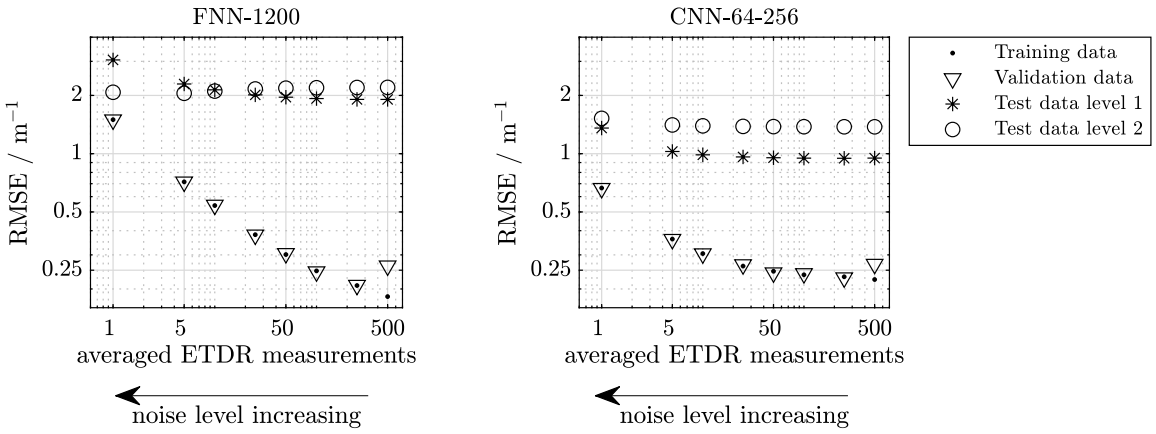

Figure 11: Input noise sensitivity of FNN-1200 and CNN-64-256

4 CONCLUSION

Spatially resolved strain sensors based on fractured CF-rovings and ETDR were first described in [6]. In this work the authors propose and evaluate a sensor design and a corresponding manufacturing process that allow strain measurement along a structure of one meter length. The use of two sensors embedded in the structure allows the measurement range to be extended to load cases with positive and negative curvature. The functionalization of the CF roving presents a major challenge when the sensors exceed the dimensions of typical specimens, since tensile tests are typically limited in length. The proposed method using a four-point bending test allows the functionalization of long structures by applying the load sectionally.

In this work, a shallow FNN and a CNN were developed, trained, and tested for their suitability to infer strain profiles. Especially for strain measurements with long sensors, a wide range of load cases must be covered within the training data to represent the loads that will occur during operation. ANNs with good generalization capabilities increase the robustness of the measurement to loads outside the range of the training data. Tests with load cases that differ from the training data as well as with noisy input data showed a better generalization ability of the CNN compared to the FNN. This makes the CNN more suitable for the inference of strain profiles from ETDR reflectograms. Furthermore, its ability to process noisy input data allows to increase the measurement rate of the system by reducing the number of ETDR measurements required per inference. For the CNN, it was found that a number of five averaged ETDR-measurements was sufficient to achieve errors similar to an input of smooth ETDR-measurements. Based on the ETDR system used, this allows measurement rates of up to 200 Hz.

The acquisition of sufficient training data and the training of ANNs for individual structures is a time consuming process, and the feasibility is strongly dependent on the ability to apply loads adequate to the expected loads in the field, while at the same time obtaining high-quality target values for the training of ANNs. Next steps in the development of CF-strain sensors for a broad applicability should therefore focus on a reproducible fabrication process of pre-functionalized sensor elements to reduce the need for individual training data.

Acknowledgements

The authors would like to thank the German Federal Ministry for Economic Affairs and Climate Action (BMWK) for funding the project MonStrain from 2021 to 2024 within the LuFo VI framework.

REFERENCES

[1] R. M. Syriac and A. B. Bhasi, "Structural health monitoring of smart composites: A review," in *Green Buildings and Sustainable Engineering*, H. Drück, R. G. Pillai, M. G. Tharian, and A. Z. Majeed, Eds. Singapore: Springer Singapore, 2019, pp. 49–59.

[2] A. H. Hartog, *An introduction to distributed optical fibre sensors*, ser. Series in fiber optic sensors. Boca Raton, FL: CRC Press Taylor & Francis Group, 2017.

[3] P. Lu, N. Lalam, M. Badar, B. Liu, B. T. Chorpening, M. P. Buric, and P. R. Ohodnicki, "Distributed optical fiber sensing: Review and perspective," *Applied Physics Reviews*, vol. 6, no. 4, p. 041302, 2019.

[4] N. Lalam and W. P. Ng, "Recent development in artificial neural network based distributed fiber optic sensors," in *2020 12th International Symposium on Communication Systems, Networks and Digital Signal Processing (CSNDSP)*. IEEE, 7/20/2020 - 7/22/2020, pp. 1–6.

[5] S. Liehr, L. A. Jäger, C. Karapanagiotis, S. Münzenberger, and S. Kowarik, "Real-time dynamic strain sensing in optical fibers using artificial neural networks," *Optics Express*, vol. 27, no. 5, pp. 7405–7425, 2019.

[6] R. Höhne, T. Ehrig, P. Kostka, and N. Modler, "Phenomenological investigation of a carbon fibre based strain sensor with spatial resolution by means of time domain reflectometry," *Materialwissenschaft und Werkstofftechnik*, vol. 47, no. 11, pp. 1024–1033, 2016.

[7] B. Oswald, H. R. Benedickter, W. Bächtold, and H. Flühler, "Spatially resolved water content profiles from inverted time domain reflectometry signals," *Water Resources Research*, vol. 39, no. 12, 2003.

[8] M. K. Smail, L. Pichon, M. Olivas, F. Auzanneau, and M. Lambert, "Detection of defects in wiring networks using time domain reflectometry," *IEEE Transactions on Magnetics*, vol. 46, no. 8, pp. 2998–3001, 2010.

[9] R. Höhne, P. Kostka, and N. Modler, "Inverse calculation of strain profiles from etdr measurements using artificial neural networks," *Journal of Sensors and Sensor Systems*, vol. 6, no. 2, pp. 389–394, 2017.

[10] J. Condé-Wolter, P. J. Steinbild, P. Kostka, T. Ehrig, A. Winkler, N. Modler, and F. Sell, "Load monitoring for sailplanes utilizing an innovative carbon fibre-based, spatially resolved strain sensorload monitoring for sailplanes utilizing an innovative carbon fibre-based, spatially resolved strain sensor," in *XXXV OSTIV CONGRESS. Congress Proceedings*, T. L. Rolf Radespiel, Ed., 2021, pp. 118–121. [Online]. Available: https://ostiv.org/congress/congress-events/congress-details/xxxv-congress-2.html?file=files/ostiv-docs/congress/2021/2021_OSTIV_Congress_proceedings.pdf

[11] ISO 14125, "Fibre-reinforced plastic composites — determination of flexural properties," Berlin, 2011-03.

[12] L. Chen, "An integral approach for large deflection cantilever beams," *International Journal of Non-Linear Mechanics*, vol. 45, no. 3, pp. 301–305, 2010.

[13] M. H. Ang, W. Wei, and L. Teck-Seng, "On the estimation of the large deflection of a cantilever beam," in *Proceedings of IECON '93 - 19th Annual Conference of IEEE Industrial Electronics*, 1993, pp. 1604–1609 vol.3.

[14] D. P. Kingma and J. Ba, "Adam: A method for stochastic optimization." [Online]. Available: https://arxiv.org/pdf/1412.6980